Journal of Power Sources 268 (2014) 269–278

Contents lists available at ScienceDirect

Journal of Power Sources

journal homepage: www.elsevier.com/locate/jpowsour

A novel iron (II) polyphthalocyanine catalyst assembled on graphene with significantly enhanced performance for oxygen reduction reaction in alkaline medium

Lin Lin, Meng Li, Liqing Jiang, Yongfeng Li, Dajun Liu, Xingquan He*, Lili Cui*

Department of Chemistry and Chemical Engineering, Changchun University of Science and Technology, Changchun 130022, PR China

HIGHLIGHTS

- FePPc/PSS-Gr is fabricated by a solvothermally assisted π–π assembling method.
- The FePPc/PSS-Gr catalyst possesses large electrochemically accessible surface area.
- Our catalyst towards ORR exhibits high catalytic activity in alkaline medium.
- The proposed catalyst towards ORR follows a direct 4-electron mechanism.

GRAPHICAL ABSTRACT

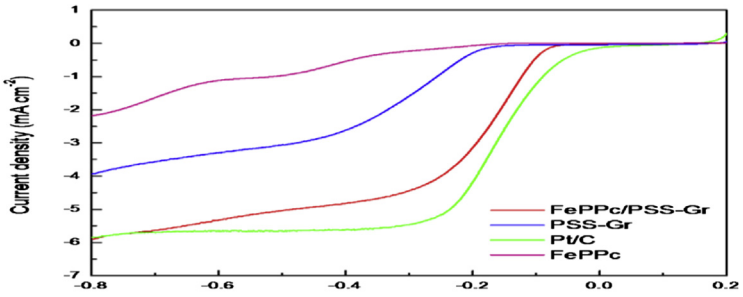

ARTICLE INFO

Article history:
Received 21 March 2014
Received in revised form
10 June 2014
Accepted 11 June 2014
Available online 18 June 2014

Keywords:
Polyphthalocyanine
Graphene
π–π interaction
Oxygen reduction reaction

ABSTRACT

To realize the large-scale commercial application of direct methanol fuel cells (DMFCs), the catalysts for oxygen reduction reaction (ORR) are the crucial obstacle. Here, an efficient non-noble-metal catalyst for ORR, denoted FePPc/PSS-Gr, has been obtained by anchoring p-phenyl-bis(3,4-dicyanophenyl) ether iron(II) polyphthalocyanine (FePPc) on poly(sodium-p-styrenesulfonate) (PSS) modified graphene (PSS-Gr) through a solvothermally assisted π–π assembling approach. The Ultraviolet–visible (UV–vis) spectroscopy, Fourier transform infrared spectroscopy (FTIR) and X-ray photoelectron spectroscopy (XPS) results reveal the π–π interaction between FePPc and PSS-Gr. The rotating disk electrode (RDE) and rotating ring disk electrode (RRDE) measurements show that the proposed catalyst possesses an excellent catalytic performance towards ORR comparable with the commercial Pt/C catalyst in alkaline medium, such as high onset potential (−0.08 V vs. SCE), half-wave potential (−0.19 V vs. SCE), better tolerance to methanol crossover, excellent stability (81.1%, retention after 10,000 s) and an efficient four-electron pathway. The enhanced electrocatalytic performance could be chiefly attributed to its large electrochemically accessible surface area, fast electron transfer rate of PSS-Gr, in particular, the synergistic effect between the FePPc moieties and the PSS-Gr sheets.

1. Introduction

Direct methanol fuel cells (DMFCs), using methanol solution or methanol steam as fuel, have many merits, including low operating temperature, reduced emission of pollutants, regeneration of the fuel and high energy density [1–3]. All of these strong points have enabled DMFCs to be used as power sources for portable electronic

* Corresponding authors. Tel.: +86 431 85583430.
E-mail address: hexingquan@hotmail.com (X. He).

http://dx.doi.org/10.1016/j.jpowsour.2014.06.062
0378-7753/

products and attracted increasing attention over the past decades. However, Pt-based materials, the best and most frequently used catalysts for oxygen reduction reaction (ORR) until now, have kept DMFCs from commercialization due to scarce reserve, low tolerance to methanol oxidation and the slow kinetics of the ORR [4–6]. Therefore, seeking for substitutes which are inexpensive, insensitive to methanol and long-term durable, is imminent. So far, various non-noble-metal catalysts have attracted immense interest, such as transition metal oxide [7–9], transition metal chalcogenides [10–13], metal-N_4 macrocycles (phthalocyanine and porphyrin) [14–17], carbon materials supported transition metal-N_4 chelate macrocycles compounds [18–22], conductive polymer-derived materials (polyaniline and polypyrrole) [23,24], heteropolyacids-based complexes [25] and heteroatom doped carbon materials [26–29].

In 1964, Jasinski reported for the first time that transition metal phthalocyanines (MPcs) showed electrocatalytic activity towards ORR [14]. Ever since, MPcs (such as iron- and cobalt- phthalocyanines) have been actively researched as candidates for ORR. Whereas, the performance of MPcs has failed to compare with Pt-based catalysts, moreover, MPcs are far from satisfying the requirements of DMFCs. The following shortcomings should be responsible for the inferior ORR capability of MPcs [22]. On the one hand, the MPc molecules are liable to aggregation so that the catalytic activity and stability reduces greatly. On the other hand, the poor electron conductivity of MPcs remains the bottleneck of facilitating electron transfer in the ORR process. To improve the ORR performance, a series of carbon nanomaterials (CNMs, such as Vulcan XC-72, carbon black, carbon nanotubes and graphene) supported MPc catalysts have been designed [18–22]. Among those carbon nanomaterials, graphene as a single layer, two-dimensional honeycombed lattice structure with sp^2 hybridized carbon atoms close-packed, has drawn tremendous attention and research interest since its first discovery in 2004, owing to its large specific surface area, good chemical and environmental stability and excellent electronic, thermodynamic and mechanical properties [30–33]. It is a promising matrix material for catalysts of the ORR. The excellent and elevated catalytic activity of the aforementioned composites might be mainly attributed to the following crucial aspects [20,22,34,35]. In the first place, CNMs can tightly anchor the MPc moieties through strong π–π interaction, improving the stability of the fabricated composite significantly. Secondly, CNMs as supports can improve the electroconductibility of the fabricated hybrids to ensure the fast electron transport capability. Thirdly, the high specific surface area of the hybrids allows the closed interaction of oxygen with amply exposed MN_x active sites during the ORR process and provides vast scale electrode-electrolyte interfaces. Last but not least, the synergistic effect between MPcs and CNMs conduces to enhance the ORR activity markedly.

Similar to phthalocyanines, the polymeric forms of phthalocyanines, so called polyphthalocyanines (PPcs), with highly conjugated π-electron system, macrocyclic hollow channel, prominent conductivity and electromagnetic properties and considerable specific surface area, have been known for a long time [36–42]. They can be employed as building blocks for a wide range of applications, such as gas sensors [39], molecular spintronic devices [39], and catalysts [40,41]. Considering the conjugated structure of MPPc with rapid electron transmission capacity and the macrocyclic hollow channel of MPPc with a large number of exposed active sites, it can be used as an electrocatalyst for ORR.

It is generally accepted that, as a conjugated system abounded with π electron, MPPc can be easily supported on the above mentioned CNMs via non-covalent π–π interaction facilitating the electron transfer process and stabilizing the systems. Herein, we fabricated a novel FePPc (molecular structure shown in Scheme 1)

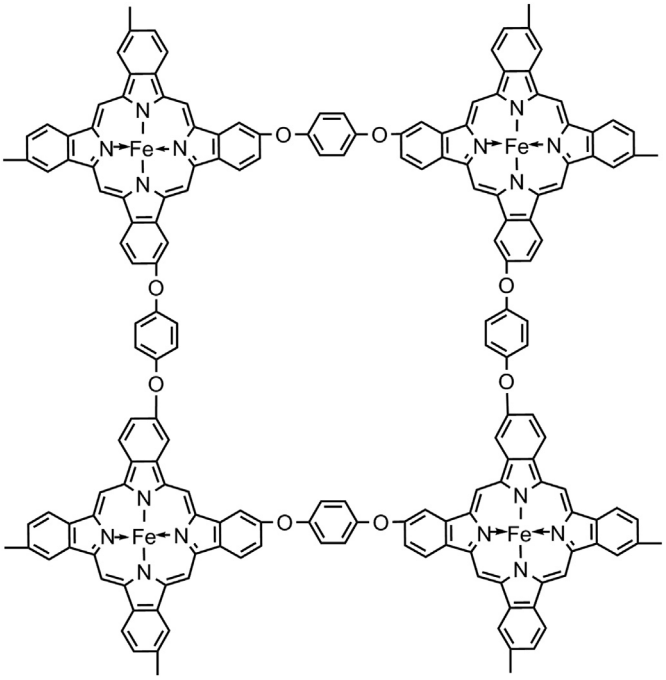

Scheme 1. Molecular structure of FePPc.

anchored on poly(sodium-p-styrenesulfonate) modified graphene (PSS-Gr) to be used as a highly efficient, methanol-tolerant, long-time stable catalyst for ORR by solvothermally assisted π–π assembling method. The FePPc/PSS-Gr composite was characterized by UV–vis, FTIR, XPS, SEM and TEM. The ORR activity, durability and stability of the FePPc/PSS-Gr catalyst were discussed in detail. The FePPc/PSS-Gr catalyst shows high catalytic activity in some respects of onset potential, half-wave potential and current density compared with Pt/C. But it exhibits superior durability, longevity and methanol-tolerance over the Pt/C catalyst. In addition, the cathode oxygen reduction reaction on the FePPc/PSS-Gr electrocatalyst in alkaline medium is unambiguous a direct four-electron reduction of oxygen to water which improves the energy efficiency.

2. Experimental

2.1. Materials

Graphite powder and 1,8-diazabicyclo [5.4.0] undec-7-ene (DBU) were purchased from Sinopharm Chemical Reagent Co., Ltd. Poly(sodium-p-styrenesulfonate) (PSS) was obtained from Sigma–Aldrich. 4-Nitrophthalonitrile was bought from Sinopharm Chemical Reagent Co., Ltd. Pt/C (20 wt %, Pt on Vulcan XC-72) was purchased from Alfa Aesar. All other reagents were analytical grade, and used without further purification, including hydroquinone, *n*-pentanol, hydrazine hydrate solution, ethanol, $NaNO_3$, $KMnO_4$, H_2O_2 and KOH. Ultra pure water was obtained from a Milli-Q water system (18.2 MΩ cm).

2.2. Sample preparation

2.2.1. Preparation of poly(sodium-p-styrenesulfonate) modified graphene (PSS-Gr)

The graphite oxide (GO) was gained from the natural graphite by a modified Hummers' method [43,44]. Poly(sodium-p-styrene

sulfonate) modified graphene (PSS-Gr) was synthesized according to the method described in our previous work [20,21].

2.2.2. Preparation of p-phenyl-bis(3,4-dicyanophenyl) ether

4-nitrophthalonitrile (6.938 g, 0.04 mol), hydroquinone (3.738 g, 0.02 mol), anhydrous potassium carbonate (5.538 g, 0.04 mol), and *N*, *N*-dimethylformamide (DMF) (20 mL) were charged into a 50 mL three-necked round-bottom flask. The mixture was heated and stirred at 55 °C for 6 h under N_2 atmosphere. Followed by slowly cooling to room temperature, the mixture was poured into distilled water to precipitate yellow powder. The crude product was washed with distilled water until neutral and then washed with ethanol until the filtrate was colorless. Finally, the solid was recrystallized in ethanol. The resulting white powder was dried in a vacuum oven at 35 °C for 24 h.

2.2.3. Preparation of p-phenyl-bis(3,4-dicyanophenyl) ether iron(II) polyphthalocyanine (FePPc)

FePPc was synthesized by a solvothermal method. A mixture of p-phenyl-bis(3,4-dicyanophenyl) ether (2 mmol, 0.7247 g), $FeCl_2 \cdot 4H_2O$ (1 mmol, 0.1988 g), 1,8-diazabicyclo [5.4.0] undec-7-ene (DBU) (0.5 mL) and *n*-pentanol (15 mL) were added into a 50 mL Teflon-lined autoclave. Then N_2 was passed into the Teflon-lined autoclave to exhaust air. At last, the Teflon-lined autoclave was sealed and maintained at 160 °C for 6 h. After cooling to room temperature, the mixture was washed with distilled water, ethanol and acetone in turn for several times. Following, the crude product was heated at 90 °C for 1 h in 1 M of HCl. Finally, the product was distilled water-washed until neutral and DMF-washed until the filtrate was colorless. The resulting green solid was dried in a vacuum oven at 35 °C for 24 h.

2.2.4. Preparation of FePPc/PSS-Gr

The FePPc/PSS-Gr composites with different mass ratios of FePPc to PSS-Gr were fabricated by a solvothermally assisted π–π assembling method. Simply, 2 mL of PSS-Gr (1 mg mL^{-1} dispersion solution in DMF), varying amounts of FePPc (2 mg, 6 mg, 10 mg, mass ratio to graphene is 1:1, 3:1 and 5:1, respectively) were dispersed in 15 mL of DMF under ultrasonic vibration for 1 h. Then, the dispersion solution was sealed in a 50 mL Teflon-lined autoclave and placed into a convection oven set at 160 °C for 12 h. Then, the vessel was allowed to return to room temperature. Finally, the mixture was centrifuged and washed with DMF, distilled water and ethanol in proper order for several times.

2.3. Characterization

Scanning electron microscopy (SEM) images were recorded by JEOL JSM-6701F electron microscope operating at 5 kV and transmission electron microscope (TEM) images were obtained using JEOLJEM-1200EX at 100 kV. The UV–vis spectrum were performed on mini UV-1240 spectrophotometer and Fourier transform infrared spectroscopy (FTIR) were collected using an FTIR-8400S spectrometer. Analysis of X-ray photoelectron spectroscopy (XPS) measurements were carried out on an ESCLAB 250 spectrometer using Al Kα as the exciting source.

2.4. Electrochemical measurements

Prior to modification, the surface of glassy carbon (GC) electrode was polished with 1.0, 0.3 and 0.05 μm α-Al_2O_3 powder slurry successively and ultrasonically rinsed with absolute ethanol and distilled water for a little while, respectively. In order to modify the GC electrode, a homogeneous ink was prepared by mixing 1.0 mg of catalyst and 1.0 mL of ethanol with the aid of ultrasonic vibration. A certain amount of the catalyst ink was dropped onto a freshly polished electrode surface to prepare a catalyst film. The catalyst loading per area on the GC electrode was kept to be 283 μg cm^{-2}.

Cyclic voltammetry (CV) was operated on a CHI 660D electrochemical workstation (Shanghai CHENHUA company) in a typical three-electrode electrochemical system consisted of a modified GC electrode (d = 3 mm), a platinum wire counter electrode and a saturated calomel reference electrode (SCE) at the scan rate of 100 mV s^{-1} in a N_2- or O_2-saturated 0.1 M KOH solution. The rotating disk electrode (RDE, d = 5 mm), current-time chronoamperometric response (i–t) and rotating ring disk electrode (RRDE, d_{disk} = 5.61 mm) measurements were carried out with a Pine Instrument Company AF-MSRCE modulator rate rotator on a CHI 660E electrochemical workstation (Shanghai CHENHUA company) using a standard three-electrode system at the scan rate of 10 mV s^{-1} in an O_2-saturated 0.1 M KOH solution. The Pt ring potential was set at 0.65 V vs. SCE to monitor the HO_2^- production in an RRDE configuration with the ring collection efficiency of 37%.

3. Results and discussion

3.1. Characterizations of FePPc/PSS-Gr composite

The morphology was investigated by means of scan electron microscopy (SEM) and transmission electron microscopy (TEM). In Fig. 1(a) and Fig. 1(b), we can see that PSS-Gr is a crumpled nanosheets structure. The PSS-Gr nanosheets get thick and the FePPc nano/micro clusters can be seen distinctly when PSS-Gr compounds with FePPc, signifying that the FePPc moieties have been successfully anchored on PSS-Gr, as seen from Fig. 1(c–h). Fig. 1(i) shows a typical TEM image of a single PSS-Gr sheet with some wrinkles on it. Fig. 1(j) displays the TEM micrograph of the composite film, the PSS-Gr nanosheets get crude and the aggregated FePPc clusters can be observed, which agrees well with the SEM results discussed above.

In an effort to better explore the π–π interaction between FePPc and PSS-Gr, UV–vis, FTIR and XPS spectra were utilized. Fig. 2(a) elucidates the UV–vis spectra of PSS-Gr (black line), FePPc (red line) and FePPc/PSS-Gr (blue line) in DMF, respectively. It can be seen that PSS-Gr shows no absorbance peak between 500 and 900 nm. FePPc exhibits a strong and sharp absorbance at 669 nm of Q band attributed to π–π* transition from the highest occupied molecular orbital (HOMO) to the lowest unoccupied molecular orbital (LUMO) of the phthalocyanine ring [42]. It also displays an additional weak vibrational satellite band at 606 nm as a result of exciton coupling between the phthalocyanine units [42]. However, the UV–vis spectrum of the FePPc/PSS-Gr composite only shows one Q band at 742 nm with a red-shift of 73 nm. The apparent bathochromic shift reflects the strong π–π interaction between FePPc and PSS-Gr.

The π–π interaction between FePPc and PSS-Gr was also investigated using FTIR measurements, which were performed on FePPc and FePPc/PSS-Gr. As shown in Fig. 2(b), the representative peaks at 1189 and 1223 cm^{-1} in the FTIR spectra of FePPc and FePPc/PSS-Gr can be assigned to Ar-O-Ar. The peaks of the FePPc/PSS-Gr composite at 1089, 1116, 1262, 1394, 1471, 1495 and 1613 cm^{-1} present absorption bands related to FePPc. The slight shifts of these peaks compared with pure FePPc, suggests the formation of a π–π bond between FePPc and PSS-Gr [21].

Fig. 2(c) presents the XPS survey spectra of GO, PSS-Gr, FePPc and FePPc/PSS-Gr, respectively. The O1s peak related to PSS-Gr declines visibly compared with GO, revealing that part of

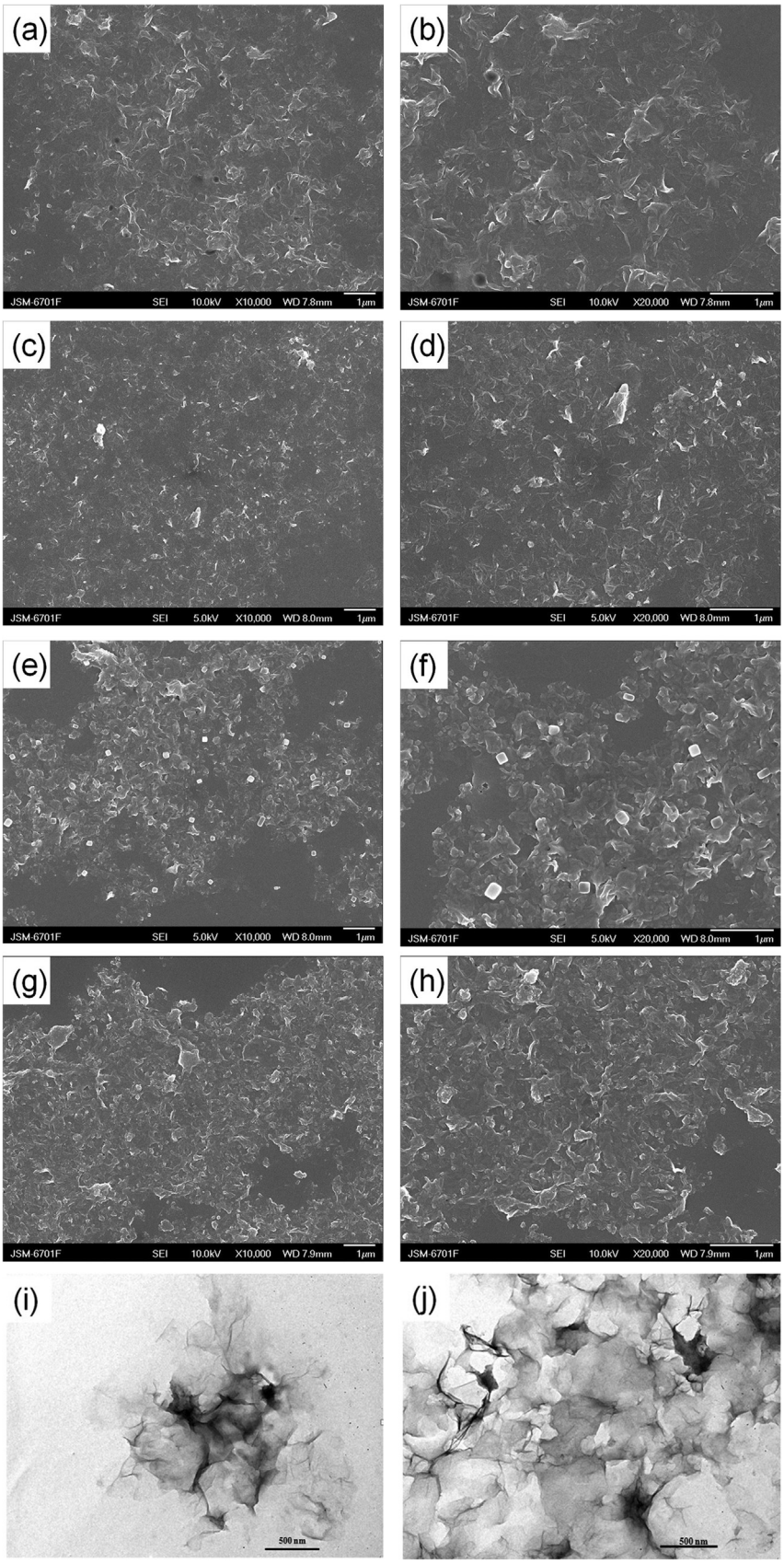

Fig. 1. SEM images of (a) and (b) PSS-Gr; (c) and (d) FePPc/PSS-Gr (1:1); (e) and (f) FePPc/PSS-Gr (3:1); (g) and (h) FePPc/PSS-Gr (5:1); (b), (d), (f) and (h) are under higher magnification; TEM images of (i) PSS-Gr and (j) FePPc/PSS-Gr (3:1).

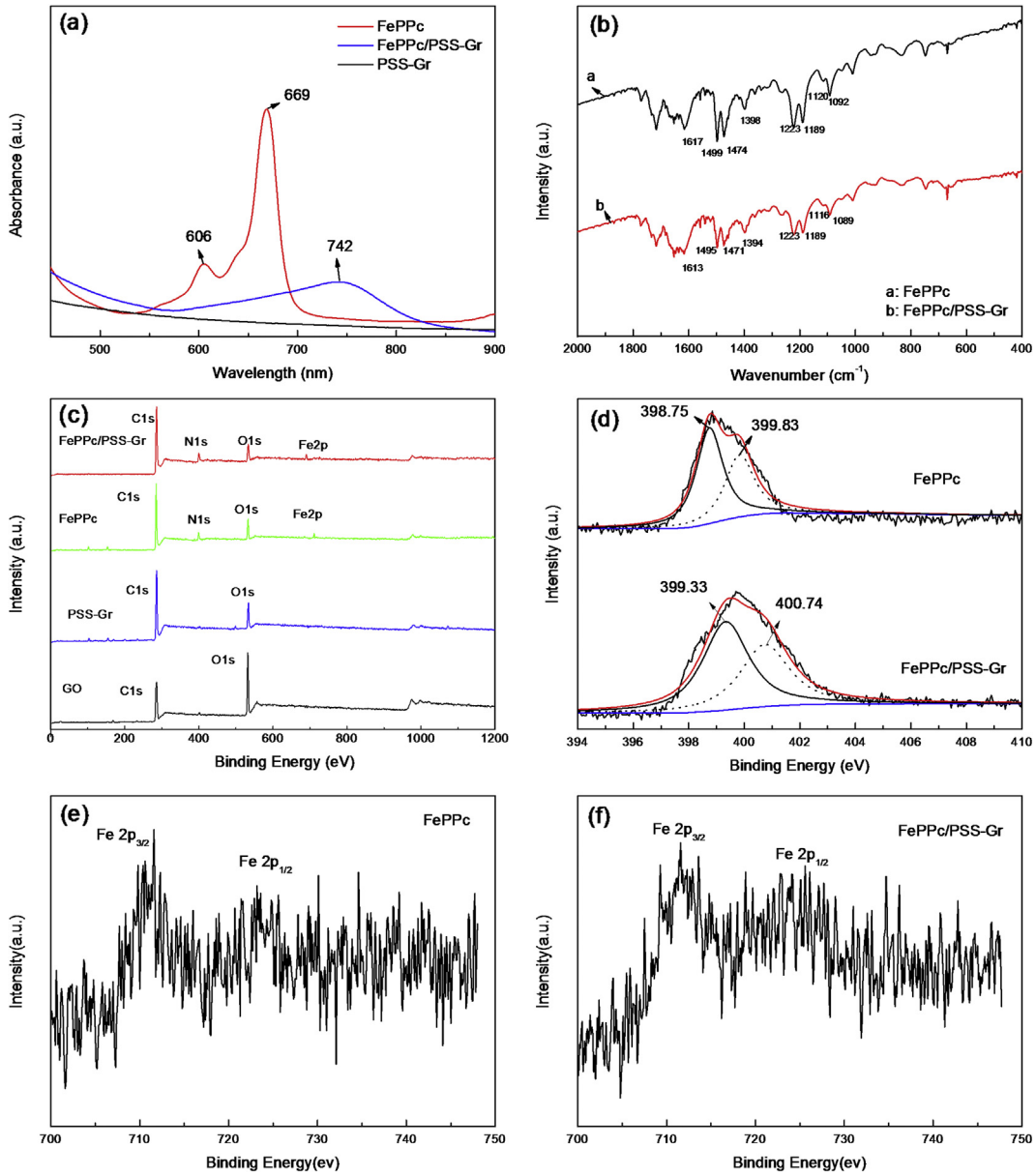

Fig. 2. (a) UV–vis absorption spectra of PSS-Gr, FePPc and FePPc/PSS-Gr (3:1); (b) FTIR spectra of FePPc and FePPc/PSS-Gr (3:1); (c) XPS spectra of FePPc/PSS-Gr (3:1), FePPc, PSS-Gr and GO; (d) High resolution N1s of XPS spectra of FePPc and FePPc/PSS-Gr (3:1); (e) High resolution Fe 2p XPS spectrum of FePPc; (f) High resolution Fe 2p XPS spectrum of FePPc/PSS-Gr.

carbon–oxygen functionalities on the surface of GO have been reduced. And from the XPS data of FePPc/PSS-Gr, the peaks of C, N, O, Fe can be observed obviously, confirming that the FePPc molecules have been successfully assembled on the PSS-Gr surface. As shown in Fig. 2(d), the deconvoluted XPS N1s spectrum of FePPc can be separated into two components centered at the binding energies of 398.75 eV (pyridinic type nitrogen) and 399.83 eV (pyrrolic type nitrogen). In contrast to FePPc, the N1s peaks of FePPc/PSS-Gr shift to higher binding energy by 0.58 and 0.91 eV for pyridine-like nitrogen and pyrrole-like nitrogen, respectively. Such higher binding energy shift manifests the charge transfer from FePPc to PSS-Gr [20]. As depicted in Fig. 2(e) and (f), the Fe $2p_{3/2}$ peak is centered at 710.6 eV, and the Fe $2p_{1/2}$ peak is located at 720.9 eV in FePPc (Fig. 2(e)). Compared with the FePPc molecule, the Fe $2p_{3/2}$ and Fe $2p_{1/2}$ values of the FePPc/PSS-Gr shifted to 711.3 and 722.2 eV, respectively (Fig. 2(f)), suggesting the interaction between graphene and FePPc leads to a decrease in the electron density on the Fe atom [22].

3.2. Catalysis of the FePPc/PSS-Gr composite for ORR

To gain insight into the relationship between the catalytic activity and the mass ratio of FePPc to PSS-Gr for ORR, we carried out the cyclic voltammetry (CV) measurements of the FePPc/PSS-Gr composites with different mass ratios of FePPc to PSS-Gr. The CV measurements of FePPc/PSS-Gr modified electrodes were performed in 0.1 M KOH solution both saturated with N_2 and O_2. As shown in Fig. 3(a), the FePPc/PSS-Gr hybrid gains the maximum peak current and more positive peak potential when the mass ratio of FePPc to PSS-Gr reaches 3:1. Therefore, the following measurements were under the condition of the best mass ratio. In Fig. 3(b), no distinguished current response can be seen when the solution is

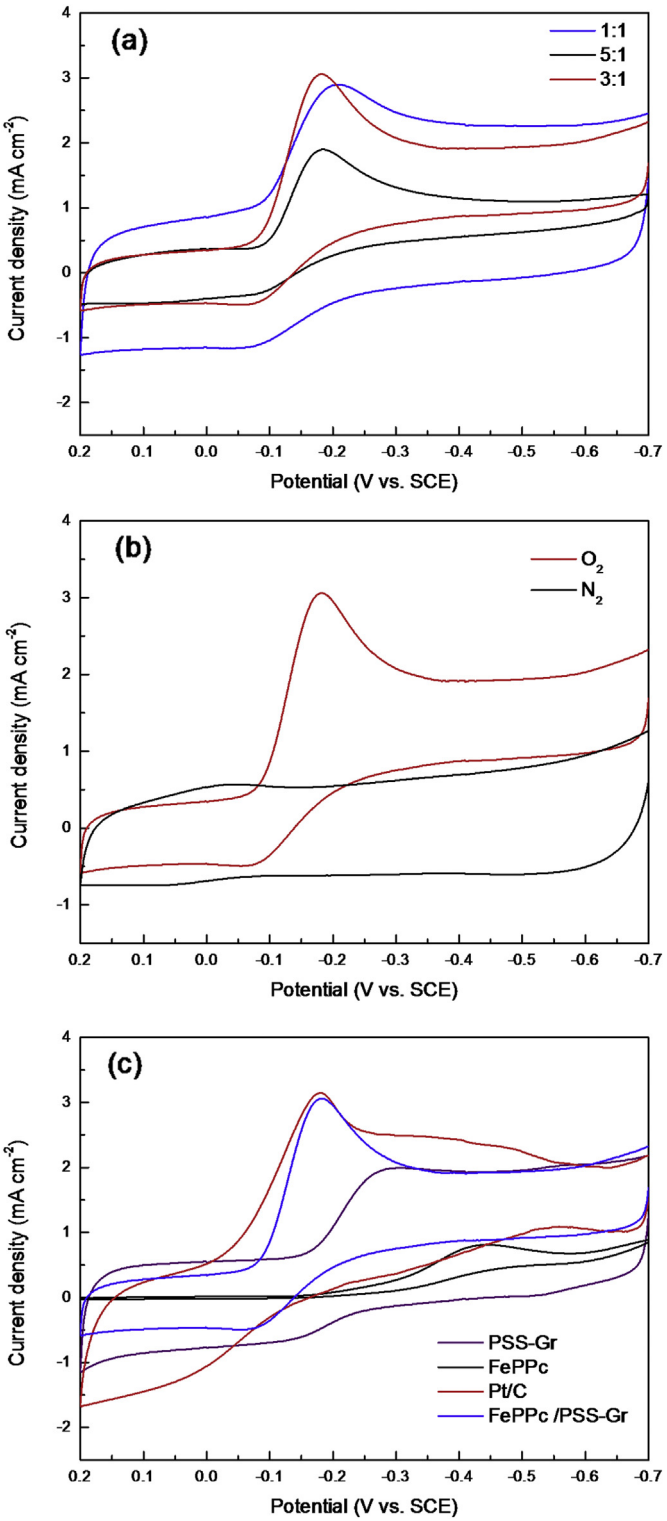

Fig. 3. CV curves of (a) FePPc/PSS-Gr with different mass ratios at the scan rate of 100 mV s^{-1} in O_2-saturated 0.1 M KOH; (b) FePPc/PSS-Gr (3:1) at the scan rate of 100 mV s^{-1} in O_2- or N_2-saturated 0.1 M KOH; (c) FePPc/PSS-Gr (3:1), FePPc, PSS-Gr and Pt/C at the scan rate of 100 mV s^{-1} in O_2-saturated 0.1 M KOH.

saturated with N_2. However, a well-defined ORR peak centered at −0.18 V vs. SCE was observed in O_2-saturated 0.1 M KOH, which reveals its electrocatalytic activity towards ORR. Then the same mass loading of different materials (FePPc, PSS-Gr and commercial 20 wt % Pt on Vulcan XC-72) were loaded on GC electrodes. As we can see in Fig. 3(c), the FePPc/PSS-Gr catalyst possesses a distinct cathodic ORR peak at −0.18 V vs. SCE, which is the same as that of Pt/C and 260 or 130 mV more positive than that of FePPc (−0.31 V vs. SCE) or PSS-Gr (−0.44 V vs. SCE). Moreover, the peak current density of the FePPc/PSS-Gr composite is much higher than that of FePPc or PSS-Gr and similar to that of Pt/C.

The electrochemically effective surface area of the electrode was estimated by cyclic voltammetry using 5 mM $Fe(CN)_6^{3-/4-}$ in 1 M KCl. The electroactive surface area can be estimated according to the Randles–Sevcik equation [16]:

$$i_p = 2.99 \times 10^5 nACD^{1/2}v^{1/2} \quad (1)$$

Where i_p is the peak current, D and C are the diffusion coefficient and bulk concentration of the redox probe (5 mM $K_3[Fe(CN)_6]$), respectively. n is the number of electrons transferred ($n = 1$), v is the scan rate. Fig. 4(b) and Fig. 4(d) demonstrate the linear relationship between the peak current (i_p) and the square root of scan rate ($v^{1/2}$), implying that the process is diffusion controlled. Moreover, as computed from Eq. (1), the electroactive surface area of FePPc/PSS-Gr modified electrode (0.1095 cm^2) is nearly 2.35 times as large as that of the polished bare GC electrode (0.0466 cm^2), which enhances the charge transfer kinetics [16].

In order to further investigate the impressive catalytic activity and the kinetics of the ORR in respect to FePPc/PSS-Gr, linear sweep voltammetry measurements on a rotating disk electrode were carried out at diverse rotation rates in O_2-saturated 0.1 M KOH with the scan rate of 10 mV s^{-1}. FePPc, PSS-Gr and Pt/C were also conducted under the same conditions for comparison. A series of polarization curves for ORR on FePPc/PSS-Gr recorded from 100 to 2500 rpm are displayed in Fig. 5(a). With increase of the rotation rates from 100 to 2500 rpm, the current density is enhanced notably due to the shortened diffusion layer [45]. Fig. 5(g) shows the RDE tests obtained on FePPc/PSS-Gr, FePPc, PSS-Gr and Pt/C, with the rotation rate of 1600 rpm in 0.1 M KOH solution saturated with O_2, and the parameters for ORR are summarized in Table 1. The ORR potential of FePPc and PSS-Gr commences at about −0.27 V and −0.18 V vs. SCE, whereas the onset potential of FePPc/PSS-Gr is positively shifted to −0.08 V vs. SCE, which is close to that of Pt/C (about −0.05 V vs. SCE). As revealed by its slightly more negative onset potential and lower current density at the low negative potential region, our catalyst is inferior to the Pt/C catalyst towards ORR, but it possesses a higher current density at the highly negative potential region, suggesting the more kinetically facile of FePPc/PSS-Gr for ORR [46]. Furthermore, the half wave potential of FePPc/PSS-Gr is slightly lower than that of Pt/C and 170 mV or 420 mV more positive than that of PSS-Gr or FePPc. So far, the active sites of CNMs-supported MPc are still under debate, but great quantities of researches have been proposed that MN_x plays an important role in the ORR process [19,34]. The prominently elevated ORR activity of the FePPc/PSS-Gr composite should be attributed to numerous exposed active sites of MN_x in FePPc. In addition, the large electrochemically effective surface area and the synergistic effect between FePPc and PSS-Gr could also promote the catalytic capability towards ORR.

It is of common knowledge that the electrochemical reduction reaction of oxygen in the cathode is a multielectron reaction and can occur via two major probable pathways: one involving the transfer of two electrons to produce H_2O_2 and HO_2^-, and the other, a direct four-electron pathway to produce H_2O and OH^- in acidic and alkaline medium, respectively. To obtain maximum energy capacity and faster oxygen reduction rate, it is highly desirable to reduce O_2 via the $4e^-$ pathway. The number of electrons transferred per

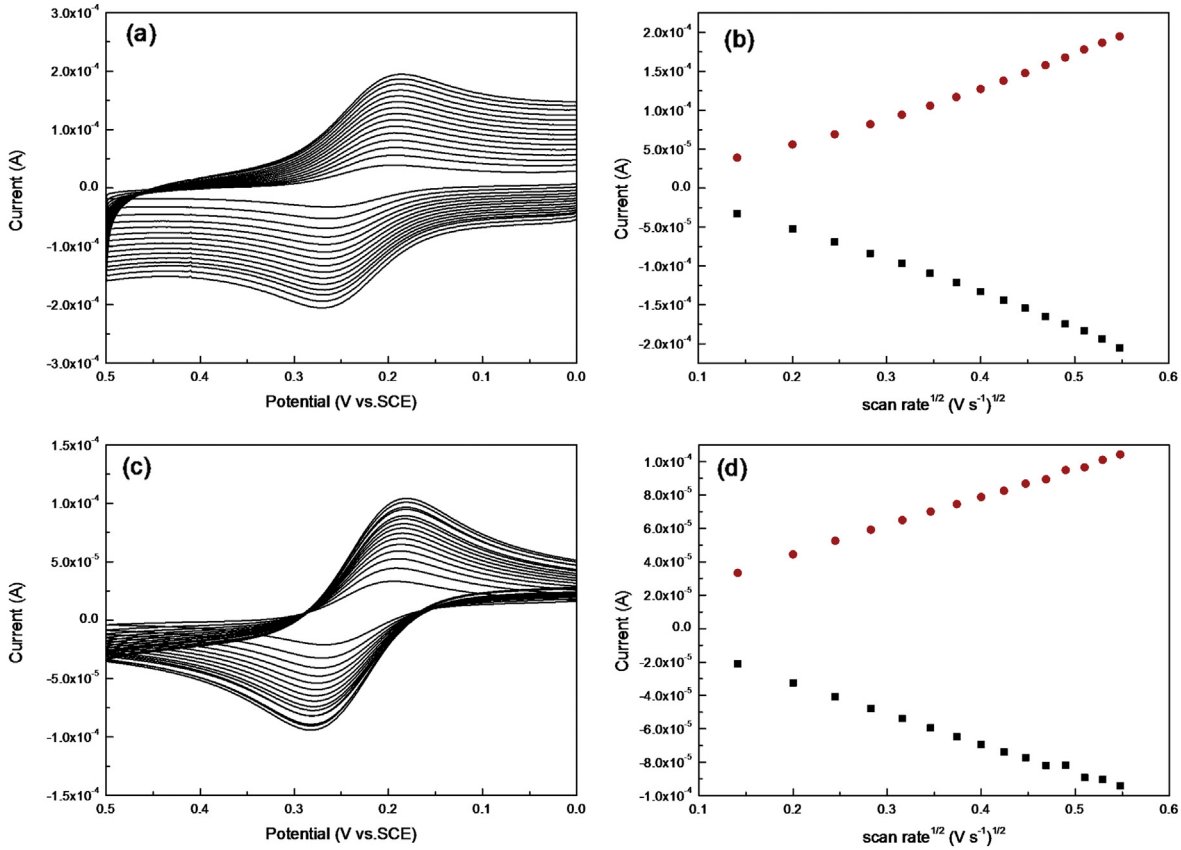

Fig. 4. CV curves of (a) FePPc/PSS-Gr (3:1) and (c) bare GC electrode in 5 mM $Fe(CN)_6^{3-/4-}$/1 M KCl at various scan rates from 20 to 300 mV s^{-1}; plots of i_p vs. $v^{1/2}$ for (b) FePPc/PSS-Gr (3:1) and (d) the polished bare GC electrode.

oxygen molecule at FePPc/PSS-Gr is further determined by the Koutechy–Levivh (K–L) equation given as follows [20]:

$$1/J = 1/J_K + 1/J_L = 1/J_K + 1/B\omega^{1/2} \quad (2)$$

$$B = 0.62nFC_0D_0^{3/2}\nu^{1/6} \quad (3)$$

$$J_k = nFKC_0 \quad (4)$$

where J represents the measured current density, J_K and J_L denote the kinetic and diffusion-limiting current densities, ω is the angular velocity of the disk ($\omega = 2\pi N$, N is the linear rotation rate), n is the overall number of electrons transferred in ORR, F is the Faraday constant ($F = 96485$ C mol^{-1}), C_0 is the bulk concentration of O_2 (1.2×10^{-6} mol cm^{-3}), D_0 is the diffusion coefficient of O_2 in 0.1 M KOH (1.9×10^{-5} cm^2 s^{-1}), ν is the kinematic viscosity of the electrolyte (0.01 cm^2 s^{-1}), and K is the electron transfer rate constant.

Fig. 5b shows the corresponding K–L plots (J^{-1} vs. $\omega^{-1/2}$) of FePPc/PSS-Gr at various potentials, which exhibit good linearity. This is an indication that the reaction is first order, and controlled by kinetics at the electrode surface as well as mass transport of oxygen molecule [47]. In addition, their slopes remain approximately constant over the potential range from −0.4 to −0.7 V vs. SCE, suggesting that the electron transfer number at different potentials is similar. Fig. 5(h) illustrates the electron transfer number within the potential range of −0.4 to −0.7 V vs. SCE for diverse catalysts. Based on the slopes of the K–L plots, the electron transfer number varies from 3.65 to 3.90 for FePPc/PSS-Gr, indicating that the ORR catalyzed on the FePPc/PSS-Gr electrode is nearly a $4e^-$ reduction process leading to OH^- as the main product, as is the case for Pt/C. Yet, the electron transfer number for PSS-Gr is about 3, a coexisting pathway involving both two-electron and four-electron process with HO_2^- as the intermediate agent.

To further verify the ORR pathway on the FePPc/PSS-Gr electrode, we performed on RRDE measurements to detect the formation of hydrogen peroxide species. The produced hydrogen peroxide species during the ORR process at the disk electrode can be monitored by the ring electrode. The percentage of hydrogen peroxide species and the electron transfer number can be determined by the following equations [48]:

$$n = (4i_D)/(i_D + i_R/N) \quad (5)$$

$$HO_2^-\% = 200 \times (i_R/N)(i_D + i_R/N) \quad (6)$$

Where i_D is the disk current, i_R is the ring current, and N is the current collection efficiency of the Pt ring. Collection efficiency ($N = 0.37$) of the ring electrode is calibrated by a $K_3Fe(CN)_6$ redox reaction in N_2-saturated 0.1 M KOH solution.

Fig. 6(a) presents the disk and ring current density for the FePPc, FePPc/PSS-Gr and Pt/C catalysts in O_2-saturated 0.1 M KOH solution. As is calculated from Eq. (5) and Eq. (6), the electron transfer number and the percentage of HO_2^- generated at different potentials on FePPc, FePPc/PSS-Gr and Pt/C are displayed in Fig. 6(b) and (c). As shown in Fig. 6(c), on both FePPc/PSS-Gr and Pt/C electrodes, no significant HO_2^- is detected, and the HO_2^- yield is negligible, which supports a 4-electron pathway to produce OH^-

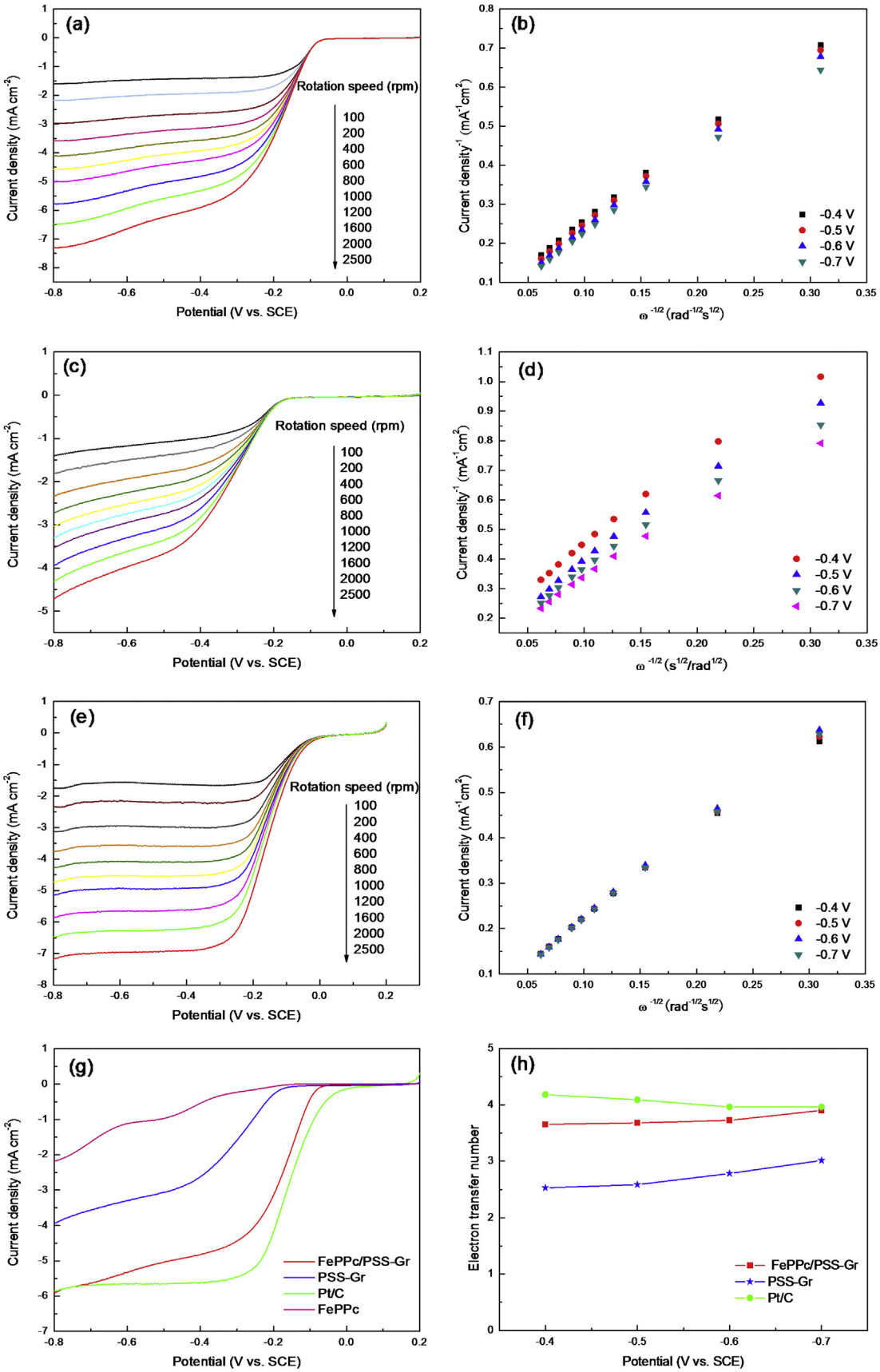

Fig. 5. LSV curves of (a) FePPc/PSS-Gr (3:1), (c) PSS-Gr and (e) Pt/C at different rotation speeds in O_2-saturated 0.1 M KOH with the scan rate of 10 mV s^{-1}; K–L plots of (b) FePPc/PSS-Gr (3:1), (d) PSS-Gr and (f) Pt/C at fixed potentials of −0.4, −0.5, −0.6 and −0.7 V; (g) LSV curves of different samples at 1600 rpm in O_2-saturated 0.1 M KOH with the scan rate of 10 mV s^{-1}; (h) The number of electrons transferred at different potentials for FePPc/PSS-Gr, PSS-Gr and Pt/C.

Table 1
Electrochemical parameters for ORR estimated from LSV.

Materials	J_L (mA cm^{-2})	Onset potential (V vs. SCE)	Half wave potential (V vs. SCE)
FePPc	2.18	−0.27	−0.58
PSS-Gr	3.93	−0.18	−0.33
FePPc/PSS-Gr	5.90	−0.08	−0.19
Pt/C	5.85	−0.05	−0.16

J_L: limiting current density at −0.8 V vs. SCE.

(calculated from Eq. (6)). And the electron transfer number of FePPc/PSS-Gr is found to vary between 3.87 and 3.93 (based on Eq. (5)) at the given potential from −0.3 to −0.7 V vs. SCE. The RRDE test is consistent with our results calculated from the K–L equation that the ORR electron transfer number for FePPc/PSS-Gr is close to 4.

The stability and methanol-tolerance have been regarded as essential points to evaluate the catalytic performance of an ORR catalyst. To examine the durability for both FePPc/PSS-Gr and Pt/C, we conducted the long-term chronoamperometric measurements with the rotation rate of 1600 rpm in 0.1 M KOH solution saturated with O_2, respectively. As depicted in Fig. 7, the FePPc/PSS-Gr catalyst exhibits a much slower attenuation with a higher current retention (81.1%) after 10000 s, whereas only 61.0% of its initial current is retained for the commercial Pt/C catalyst, demonstrating the remarkable stability of our catalyst. In DMFCs, crossover of methanol from anode to cathode can bring about the loss of equilibrium electrode potential and poisoning of catalyst when the methanol is oxidized. Thus, a good electrocatalyst must be inert to methanol oxidation. On the matter, the tests on FePPc/PSS-Gr and Pt/C were evaluated in an O_2-saturated 0.1 M KOH solution with 3 M methanol (Fig. 8), respectively. As pictured in Fig. 8(a), after 3 M methanol was added, the cathodic peak for ORR vanishes, whereas a new peak of methanol oxidation at 0.06 V vs. SCE appears, indicating a strong crossover effect on Pt/C. In contrast, the cathodic peak current of FePPc/PSS-Gr for ORR declines slightly and the peak potential scarcely changes in the CV curve of FePPc/PSS-Gr in Fig. 8(b). These results certainly highlight that the FePPc/PSS-Gr catalyst has excellent methanol-tolerance compared with Pt/C. The insensitivity to methanol enables FePPc/PSS-Gr to be utilized as a substitute for Pt/C towards ORR in DMFCs.

4. Conclusions

In summary, a novel iron (II) polyphthalocyanine (FePPc) was synthesized and then an efficient ORR catalyst was obtained through anchoring FePPc onto PSS-Gr via solvothermally assisted π–π assembling method. SEM and TEM results demonstrate that FePPc have been successfully anchored on PSS-Gr. XPS, FTIR and UV–vis spectra analyzes confirm the charge transfer from FePPc to PSS-Gr and the forceful π–π interaction between FePPc and PSS-Gr. Electrochemical measurements manifest that the FePPc/PSS-Gr catalyst offers exceptional catalytic activity for ORR, which should be ascribed to its large electrochemically accessible surface area and the synergistic effect between FePPc and PSS-Gr. Compared with the Pt/C catalyst, the FePPc/PSS-Gr catalyst possesses much higher selectivity, stability and a considerable reduced methanol crossover effect. In addition, the FePPc/PSS-Gr hybrid affords a facile 4-electron pathway for ORR which maximizes energy efficiency. In a word, the FePPc/PSS-Gr catalyst is a promising ORR candidate in alkaline medium for DMFCs.

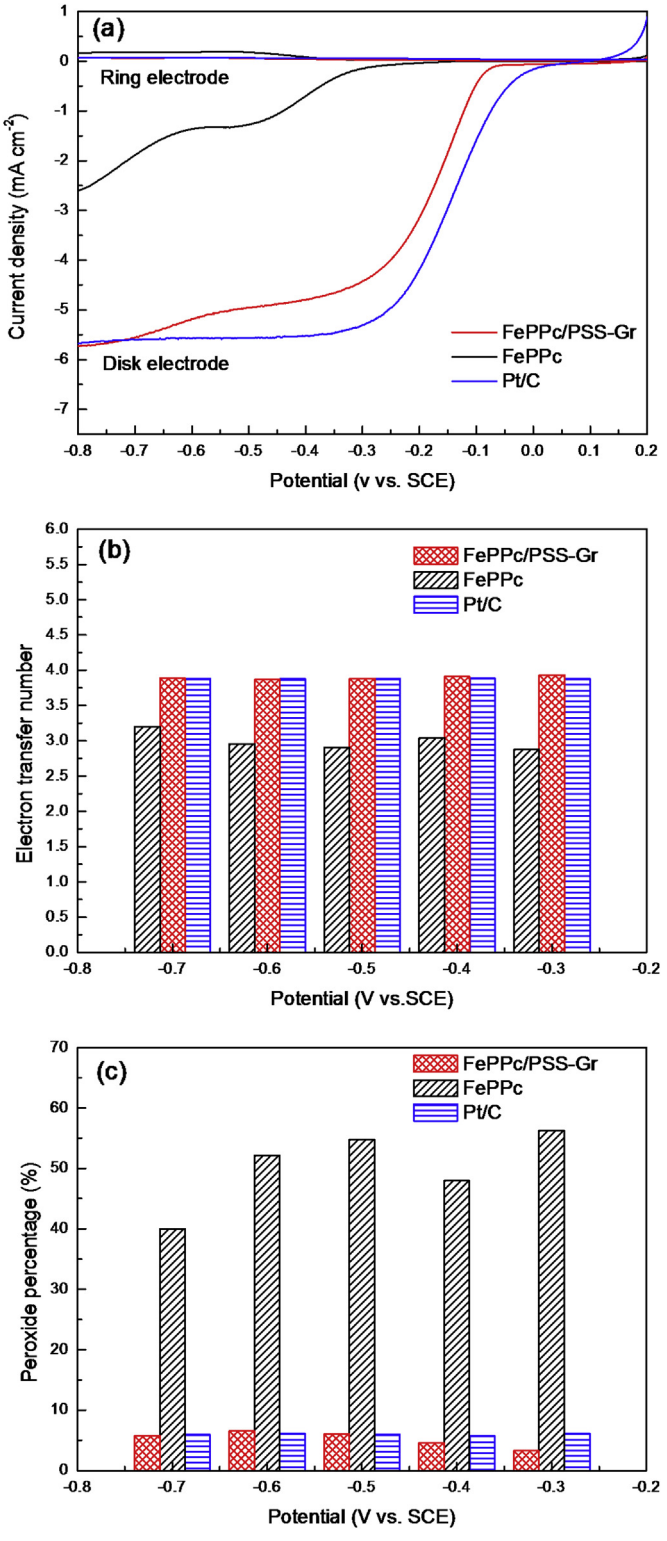

Fig. 6. (a) RRDE tests of the ORR on FePPc, FePPc/PSS-Gr and Pt/C in O_2-saturated 0.1 M KOH at the rotation speed of 1600 rpm and at the scan rate of 10 mV s^{-1}. The ring electrode is polarized at 0.65 V vs. SCE; (b) Electron transfer number and (c) peroxide percentage of FePPc, FePPc/PSS-Gr and Pt/C.

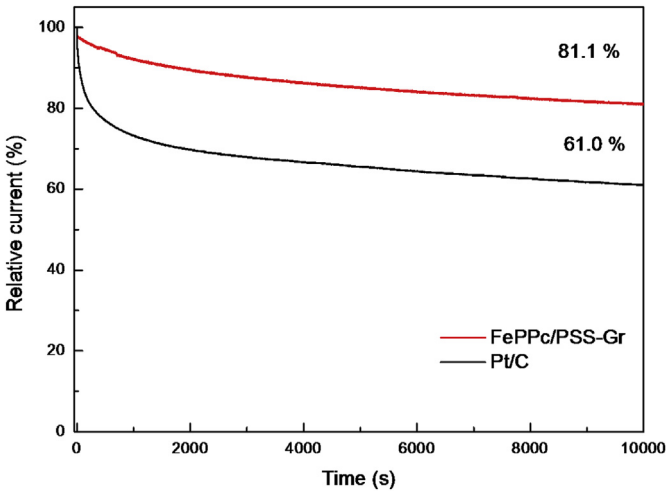

Fig. 7. The *i*–*t* curves of the FePPc/PSS-Gr and commercial Pt/C catalysts at −0.21 V and −0.20 V in O_2-saturated 0.1 M KOH with the rotation speed of 1600 rpm.

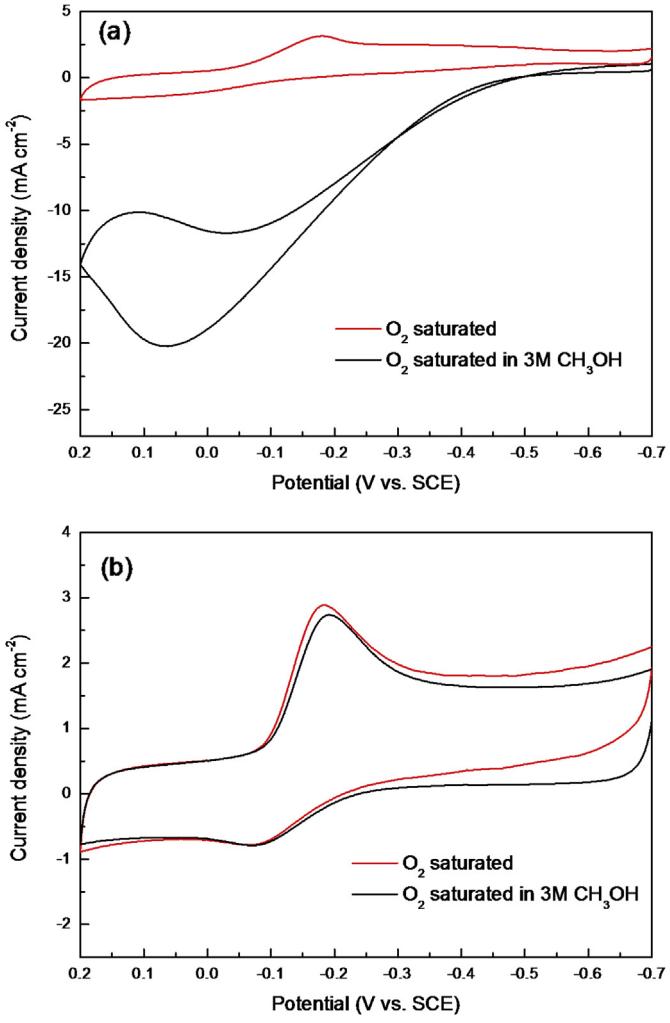

Fig. 8. CV curves of (a) Pt/C and (b) FePPc/PSS-Gr (3:1) at the scan rate of 100 mV s^{-1} in O_2-saturated 0.1 M KOH solution with and without 3 M CH_3OH.

Acknowledgments

This research has been financed by the National Natural Science Foundation of China (No. 21273024) and Natural Science Foundation of Jilin Province, China (No. 201215135).

References

[1] C. Coutanceau, R.K. Koffi, J.-M. Léger, K. Marestin, R. Mercier, C. Nayoze, P. Capron, J. Power Sources 160 (2006) 334–339.
[2] A.S. Gago, D. Morales-Acosta, L.G. Arriaga, N. Alonso-Vante, J. Power Sources 196 (2011) 1324–1328.
[3] L. Zhang, J.J. Zhang, D.P. Wilkinson, H.J. Wang, J. Power Sources 156 (2006) 171–182.
[4] M. Winter, R.J. Brodd, Chem. Rev. 104 (2004) 4245–4270.
[5] A. Rabis, P. Rodriguez, T.J. Schmidt, ACS Catal. 2 (2012) 864–890.
[6] D.S. Su, G.Q. Sun, Angew. Chem. Int. Ed. 50 (2011) 11570–11572.
[7] S.V. Mentus, Electrochim. Acta 50 (2004) 27–32.
[8] Y. Gorlin, T.F. Jaramillo, J. Am. Chem. Soc. 132 (2010) 13612–13614.
[9] Y.Y. Liang, Y.G. Li, H.L. Wang, J.G. Zhou, J. Wang, T. Regier, H.J. Dai, Nat. Mater. 10 (2011) 780–786.
[10] N. Alonso-Vante, H. Tributsch, Nature 323 (1986) 431–432.
[11] R.W. Reeve, P.A. Christensen, A. Hamnett, S.A. Haydock, S.C. Roy, J. Electrochem. Soc. 145 (1998) 3463–3471.
[12] N. Alonso-Vante, P. Bogdanoff, H. Tributsch, J. Catal. 190 (2000) 240–246.
[13] Y.J. Feng, T. He, N. Alonso-Vante, Fuel Cells 10 (2010) 77–83.
[14] R. Jasinski, Nature 201 (1964) 1212–1213.
[15] W.M. Li, A.P. Yu, D.C. Higgins, B.G. Lianos, Z.W. Chen, J. Am. Chem. Soc. 132 (2010) 17056–17058.
[16] M. Jahan, Q.L. Bao, K.P. Loh, J. Am. Chem. Soc. 134 (2012) 6707–6713.
[17] R. Baker, D.P. Wilkinson, J.J. Zhang, Electrochim. Acta 54 (2009) 3098–3102.
[18] X.M. Hu, D.G. Xia, L. Zhang, J.J. Zhang, J. Power Sources 231 (2013) 91–96.
[19] G.Q. Mo, S.Y. Liao, Y.Z. Zhang, W.D. Zhang, J.S. Ye, Electrochim. Acta 76 (2012) 430–439.
[20] L.L. Cui, G.J. Lv, Z.Y. Dou, X.Q. He, Electrochim. Acta 106 (2013) 272–278.
[21] G.J. Lv, L.L. Cui, Y.Y. Wu, Y. Liu, T. Pu, X.Q. He, Phys. Chem. Chem. Phys. 151 (2013) 13093–13100.
[22] Y.Y. Jiang, Y.Z. Lu, X.Y. Lv, D.X. Han, Q.X. Zhang, L. Niu, W. Chen, ACS Catal. 3 (2013) 1263–1271.
[23] G. Wu, K.L. More, C.M. Johnston, P. Zelenay, Science 332 (2011) 443–447.
[24] R. Bashyam, P. Zelenay, Nature 443 (2006) 63–66.
[25] R.J. Stanis, M.-C. Kuo, A.J. Rickett, J.A. Turner, A.M. Herring, Electrochim. Acta 53 (2008) 8277–8286.
[26] Z.Y. Lin, G. Waller, Y. Liu, M.L. Liu, C.-P. Wong, Adv. Energy Mater. 2 (2012) 884–888.
[27] Z.H. Sheng, H.L. Gao, W.J. Bao, F.B. Wang, X.H. Xia, J. Mater. Chem. 22 (2012) 390–395.
[28] Z. Yang, Z. Yao, G.F. Li, G.Y. Fang, H.G. Nie, Z. Liu, X.M. Zhou, X.A. Chen, S.M. Huang, ACS Nano. 6 (2012) 205–211.
[29] C.H. Choi, M.W. Chung, H.C. Kwon, S.H. Park, S.I. Woo, J. Mater. Chem. A 1 (2013) 3694–3699.
[30] K.S. Novoselov, A.K. Geim, S.V. Morozov, D. Jiang, Y. Zhang, S.V. Dubonos, I.V. Grigorieva, A.A. Firsov, Science 306 (2004) 666–669.
[31] A.K. Geim, K.S. Novoselov, Nat. Mater. 6 (2007) 183–191.
[32] M.J. Allen, V.C. Tung, R.B. Kaner, Chem. Rev. 110 (2010) 132–145.
[33] S.J. Guo, S.J. Dong, Chem. Soc. Rev. 40 (2011) 2644–2672.
[34] Z.S. Wu, L. Chen, J.Z. Liu, K. Parvez, H.W. Liang, J. Shu, H. Sachdev, R. Graf, X.L. Feng, K. Müllen, Adv. Mater. 25 (2013) 6879–6883.
[35] H.J. Tang, H.J. Yin, J.Y. Wang, N.L. Yang, D. Wang, Z.Y. Tang, Angew. Chem. Int. Ed. 52 (2013) 5585–5589.
[36] R. Bannehr, G. Meyer, D. Wöhrle, Polym. Bull. 2 (1980) 841–846.
[37] N.B. McKeown, J. Mater. Chem. 10 (2000) 1979–1995.
[38] M. Abel, S. Clair, O. Ourdjini, M. Mossoyan, L. Porte, J. Am. Chem. Soc. 133 (2011) 1203–1205.
[39] H.B. Jiang, M.L. Bai, P. Wei, L.L. Sun, Z.Y. Shen, S.M. Hou, Sensors 12 (2012) 8438–8446.
[40] Q.M. Deng, L.N. Zhao, X.F. Gao, M. Zhang, Y.H. Luo, Y.L. Zhao, Small 9 (2013) 3506–3513.
[41] G.F. Xu, Z.F. Li, S.W. Wang, X.J. Yu, J. Power Sources 195 (2010) 4731–4735.
[42] İ. Değirmencioğlu, R. Bayrak, M. Er, K. Serbest, Dyes Pigm. 83 (2009) 51–58.
[43] W.S. Hummers, R.E. Offeman, J. Am. Chem. Soc. 80 (1958) 1339.
[44] L.J. Cote, F. Kim, J.X. Huang, J. Am. Chem. Soc. 131 (2009) 1043–1049.
[45] W. Yang, T.-P. Fellinger, M. Antonietti, J. Am. Chem. Soc. 133 (2011) 206–209.
[46] Z.J. Jiang, Z.Q. Jiang, W.H. Chen, J. Power Sources 251 (2014) 55–65.
[47] A. Morozan, S. Campidelli, A. Filoramo, B. Jousselme, S. Palacin, Carbon 49 (2011) 4839–4847.
[48] Y. Liu, Y.Y. Wu, G.J. Lv, T. Pu, X.Q. He, L.L. Cui, Electrochim. Acta 112 (2013) 269–278.